Automotive Experiences
Vol. 6 No. 2 (2023) pp. 273-289
p-ISSN: 2615-6202 e-ISSN: 2615-6636

Research Paper

Application of a PEM Fuel Cell Engine as a Small-Scale Power Generator for Small Cars with Different Fuel Concentrations

Yusuf Dewantoro Herlambang[1], **Wahyu Sulistiyo**[2], **Margana**[1], **Nanang Apriandi**[1], **Marliyati**[3], **Muji Setiyo**[4], **Jin Cherng Shyu**[5]

[1]Department of Mechanical Engineering, Politeknik Negeri Semarang, Semarang 50275, Indonesia
[2]Department of Electrical Engineering, Politeknik Negeri Semarang, Semarang 50275, Indonesia
[3]Department of Accounting, Politeknik Negeri Semarang, Semarang 50275, Indonesia
[4]Department of Mechanical Engineering, Universitas Muhammadiyah Magelang, Magelang 56172, Indonesia
[5]Department of Mechanical Engineering, National Kaohsiung University of Science and Technology, Kaohsiung 80778, Taiwan

masyusufdh@polines.ac.id

https://doi.org/10.31603/ae.9225

Check for updates

Published by Automotive Laboratory of Universitas Muhammadiyah Magelang collaboration with Association of Indonesian Vocational Educators (AIVE)

Article Info
Submitted:
01/06/2023
Revised:
27/07/2023
Accepted:
01/08/2023
Online first:
27/08/2023

Abstract

A fuel cell power generation system is a renewable energy system that works based on electrochemical processes and produces a direct electric current (DC). Specifically, Proton Exchange Membrane (PEM) Fuel Cell can operate at low temperatures and produce an efficiency of around 40-60%. In this study, the performance test of the PEM Fuel Cell for power generation was carried out by supplying hydrogen gas using hydrogen from the electrolysis of the hydrogen generator with a variation of KOH catalyst solution with a concentration of 0.5 M; 1.0 M; 1.5 M; 2 M and using Ultra High Purity (UHP) hydrogen with various flow rates of 250 mL/min, 300 mL/min, 350 mL/min, 400 mL/min, 450 mL/min, and 500 mL/min. The test results showed that the output power of hydrogen produced by the electrolysis process was 10.8 W at a concentration of 1 M solutions at an input current of 20 A. The greater the concentration of the catalyst solution, the smaller the electrical power required for the electrolysis process. However, the hydrogen power supply produced by the hydrogen generator was not optimal, so it did not meet the needs of the PEM Fuel Cell. As a result, the PEM Fuel Cell could not work. Meanwhile, testing with UHP hydrogen produced the highest electrical power of 31.588 W at a flow rate of 450 mL/min with a load of 20 W. It indicates that the PEM Fuel Cell is optimal at the output power value with an efficiency of 69.80%.

Keywords: PEM Fuel Cell; Hydrogen generator; Power engines; Ultra-high purity; Efficiency

1. Introduction

Renewable energy is crucial in meeting energy needs considering that the source is abundant. It is because using fuel for conventional power plants in the long term can deplete fossil fuels and also cause environmental pollution [1]–[3]. In this regard, Indonesia already has an energy mix target for electricity generation by utilizing New Renewable Energy (NRE) by 23% in 2025 and 31% in 2050. Until the end of 2018, the proportion of NRE mix in power plants was still around 14% or 9 GW. In fact, Indonesia has an enormous NRE potential, reaching more than 440 GW. The potential includes geothermal, wind, solar, water, and others [4]. Despite the abundant potential, unfortunately, the utilization of NRE has not been maximized. Moreover, Indonesia has significant challenges in realizing this potential because the addition of NRE generating capacity is relatively slow compared to fossil energy.

One of the efforts as an energy source solution for the future is the fuel cell. The fuel cell is an electrochemical device that converts chemical energy as fuel into electrical energy directly,

which is quite promising as a generator with high efficiency and low environmental impact [5]–[8]. The fuel cell is also an electrochemical technology fueled by hydrogen, continuously converting chemical energy into electrical energy as long as there are fuel and oxidizing agents. One type of fuel cell is the Proton Exchange Membrane Fuel Cell (PEMFC). PEM Fuel Cell is a device that uses hydrogen gas or hydrogen-rich fuel and oxygen (air) to generate electricity through an electrochemical process without burning fuel [9]–[11].

The working principle of the PEM Fuel Cell is to convert hydrogen into electrical energy by breaking hydrogen into proton and electron configurations carried out by a catalyst. Protons flow through the membrane, and electrons flow through the current collector to produce a direct electric current [12]. Then, the protons and electrons from the hydrogen react with the air to produce water. Some of the factors that influence this process are the flow rate and quality of the hydrogen fuel produced by the hydrogen generator and the output capacity of the fuel cell itself [13]–[16].

In previous studies on the performance of the PEM Fuel Cell, application development of fuel cells and modification of fuel cells produce greater power so that they can be used more widely [17]–[19]. Modification of the tool is an action to change, replace, and repair certain parts. Modifications are made to improve the performance of the PEM Fuel Cell. On the other hand, applications of fuel cells range from transportation and portable power tools to power sources for residential use [20], [21]. Application of the PEM Fuel Cell was with nominal operating output specifications of 150-170 W. In addition, modifications were made to test the fuel cell by adding a digital voltmeter amperemeter, SCC (Solar Charge Controller), pressure gauge, rotameter, reservoir H_2, and changing the load, which were applied by [22], [23]. The modification is also based on the less-than-optimal hydrogen fuel produced by the hydrogen generator by electrolysis so that the fuel supply is switched to UHP (Ultra High Purity) Hydrogen with a purity level of 99.999% [24]–[26].

Hydrogen (H_2) is produced from crude oil or natural gas by cracking or steam reforming process in a reactor or by electrolysis of water into H_2 and O_2. High Purity (HP) & Ultra High Purity (UHP) hydrogen are special gases produced by multiple filtration and purification systems [27]–[30]. Moreover, the purity level is controlled very carefully and it uses various analytical tools. Hydrogen gas also comes in various grades: Welding Grade Hydrogen Gas 99.96%, High Purity Hydrogen Gas 99.99%, and Ultra High Purity Hydrogen Gas 99.99%. In this case, hydrogen gas UHP 99.99% has a very high level of purity, often used for the needs of laboratories and power generation companies. The novelty of this study investigates the application of a PEM fuel cell engine through a simulation model of the PEM fuel cell and experimentally through testing a fuel cell engine. A three-dimensional flow simulation of a PEM fuel cell has been presented. Computational analysis of the model shows how to modify the fuel cell to incorporate the required electrochemical processes. The diffusion layers at the anode and cathode show a significant difference from studies that do not include the diffusion layer. In addition, it also analyzes the value of SFC to determine the performance of a fuel cell engine which can describe the ratio between the amount of hydrogen gas fuel consumption and the electrical energy produced by a fuel cell engine.

2. Methods

2.1. Computational Simulation Model

The schematic illustrates the computation domain and geometry of the microfluidic fuel cell, as shown in **Figure 1** and the value of the simulation parameters is given in **Table 1**. The PEM fuel cell having a 20-mm-long, 1-mm-wide, and 1-mm-high cell channel was numerically investigated at volumetric flow rates 0.5 mL/min.

In **Figure 1**, the serpentine channel model using a set of conservation equations is developed and solved numerically to investigate the gas channel geometrical effect such as the shape of gas channel cross-section and its convergence and shoulder area width on cell performance and transport phenomena. The equations which formulate the mass, momentum, and species conservation within the channel, the porous gas diffusion layer, and catalyst layer, along with the electrochemical reaction on the catalyst layer are simultaneously solved with appropriate boundary conditions under steady-state [24]–[26].

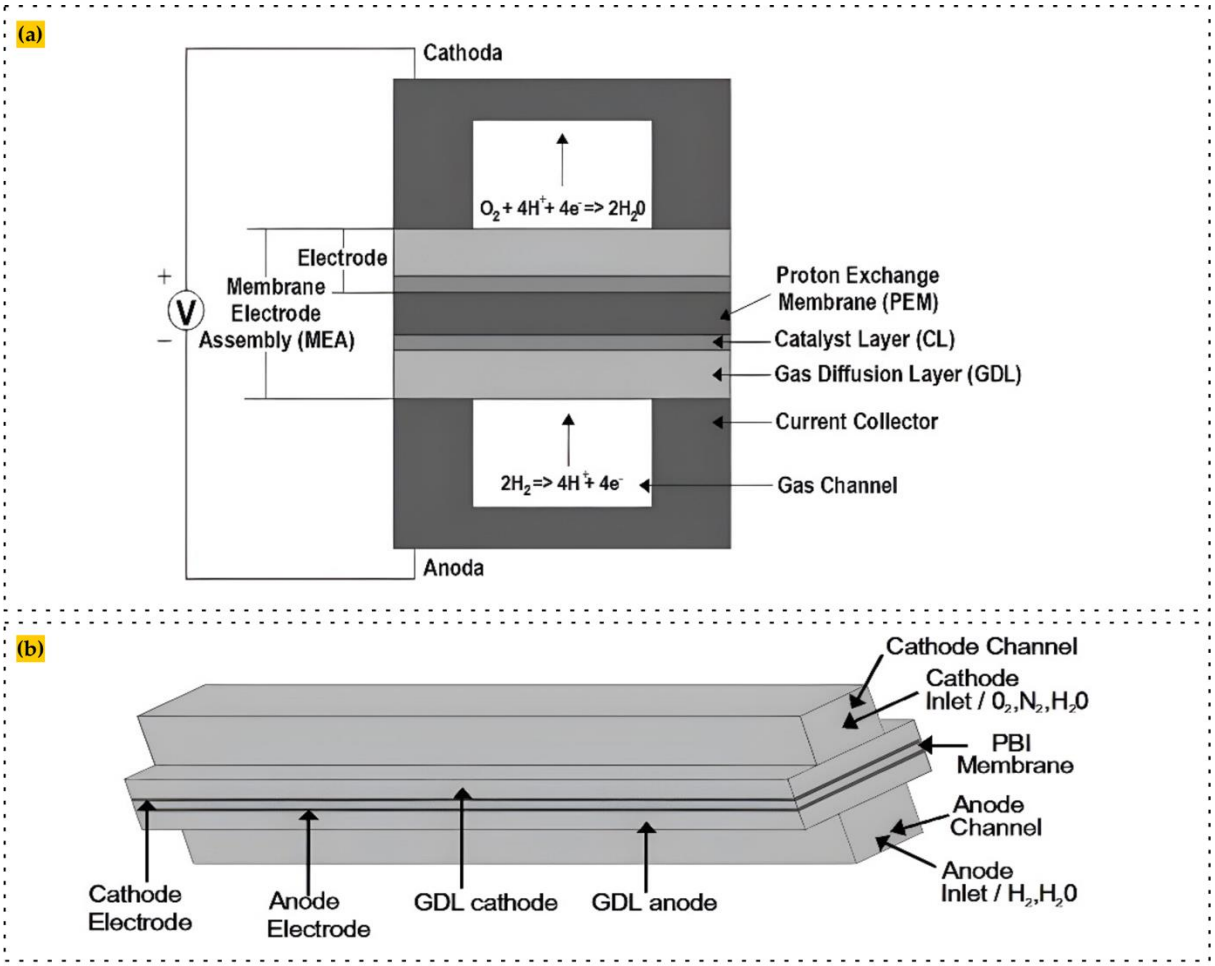

Figure 1. Geometry of PEM fuel cell (a) the flow channel fuel cell and boundaries of the computational domain; (b) 3-D computational model a single cell of PEM fuel cell

Table 1. The value of the simulation parameters

Parameters	Value
Cell length	0.02 m
Channel height	0.001 m
Channel width	0.001 m
GDL width	380 E-6 m
Porous electrode thickness	50 E-6 m
Membrane thickness	100 E-6 m
GDL porosity	0.4 [4]
GDL permeability	1.18 E-11 m^2
GDL electric conductivity	222 S/m [11]
Anode inlet flow velocity	0.2 m/s
Cathode inlet flow velocity	0.5 m/s
Anode viscosity	1.19 E-5 Pa.s
Cathode viscosity	2.46 E-5 Pa.s
Cell temperature	303 K
Reference pressure	101 E3 Pa
Cell voltage	0.9 V
Oxygen reference concentration	50 mol/m^3
Hydrogen reference concentration	50 mol/m^3
Membrane conductivity	9.825 S/m [17]
Volumetric flow rate	0.5 mL/min
Cathode charge transfer coefficient	2 [31]
Anode charge transfer coefficient	0.5 [31]

A 3-D numerical simulation model was performed based on the following assumptions and boundary conditions:

a. Fuel cell system is three-dimensional, isothermal domain, steady-state, laminar flow, and incompressible;
b. The electrodes are considered as an isotropic porous media and homogeneous;
c. Fuel crossover in the cathode reaction is considered;
d. Oxygen transport in the porous air-breathing cathode is by diffusion only;
e. Product carbon dioxide is fully dissolved in the solution;
f. The porous media flow in the GDL (Gas Diffusion Layer) was described by Brinkman equation;
g. Electrochemical reaction take place at 300 K, 1 atm which is governed by Butler-Volmer kinetics to get the V-I and P-I curves.
h. No-slip boundary condition is set for all the walls. So, the velocity for all channel walls is equal to zero.

A set of the steady state conservation equation is used to govern the computational domain in 3-D Cartesian coordinates which were formulated with continuity equation and momentum equation, species transport equation, and charge equation are given as Eq. (1), Eq. (2), Eq. (3) and Eq. (4), respectively.

$$\rho(\nabla \cdot \vec{u}) = 0 \tag{1}$$

$$\rho(\vec{u} \cdot \nabla\vec{u}) = -\nabla p + \mu(\nabla^2\vec{u} + (\nabla^2\vec{u})^T) \tag{2}$$

$$\nabla \cdot (-D\nabla c + c\vec{u}) = 0 \tag{3}$$

$$\sigma\nabla \cdot \nabla\varphi = 0 \tag{4}$$

where $\vec{u}$, ρ, μ, p, c, D, σ_s, φ_s are the velocity vector, the fluid density, fluid viscosity, static pressure, the local concentration of the species in the anode and cathode, the diffusion coefficient of species, the electronic/electrolyte conductivity, and the over potential in catalyst layer/electrolyte. Brinkman equation includes the porosity in the permeability of the porous media which are used to account the consumption of the species (Eq. 5).

Based on Eq. (5), ε is the porosity of the media, k is the permeability of the electrodes (catalyst layers and gas diffusion layers/porous electrodes). The rate of the reaction is controlled merely by the rate of the electrochemical charge transfer, as follows Eq. 6 [27], [28].

Based on Eq. (6), $i_{loc,a}$ represents the local current density in the anode, a is the density of catalytic active area $(a = 1)$, $i_{0,f}$ is exchange current density at the anode, C_f is the local fuel concentration, $C_{f,ref}$ is the reference fuel concentration, β is the reaction order $(\beta = 1)$, α_a and α_c is the charge transfer coefficients, R is the ideal gas constant, T is absolute temperature, and η is the activation over potential on the electrodes to overcome irreversibilities [27], which is determined by Eq. (7).

Based on Eq. (7), φ_s and φ_l are the electric potential of anode catalyst layer and the local electrolyte potential derived from Eq. (4), E_{eq} represents the equilibrium potential (reversible). In order to properly the electrochemical reaction in the cathode, fuel crossover is considered in the microfluidic fuel cells. The rate of reaction for the cathode is calculated by the following Eq. (8) [28]–[30].

Based on Eq. (8), $i_{loc,c}$ represents the local current density in the cathode, $i_{0,o}$ is exchange current density at the cathode, C_o is the local oxygen concentration, $C_{o,ref}$ is the reference oxygen concentration, and η is the activation over potential on the electrodes to overcome irreversibilities.

$$\frac{\rho}{\varepsilon^2}(\vec{u} \cdot \nabla\vec{u}) = -\nabla p - \frac{\mu}{k}\vec{u} + \nabla\left(\frac{\mu}{\varepsilon}(\nabla\vec{u} + (\nabla\vec{u})^T) - \frac{2}{3}\frac{\mu}{\varepsilon}(\nabla \cdot \vec{u})I\right) \tag{5}$$

$$i_{loc,a} = i_{0,f}\left(\frac{C_f}{C_{f,ref}}\right)^{\beta}\left[exp\left(\frac{\alpha_a nF}{RT}\eta\right) - exp\left(\frac{\alpha_c nF}{RT}\eta\right)\right] \tag{6}$$

$$\eta_a = \varphi_s - \varphi_l - E_{eq} \tag{7}$$

$$i_{loc,c} = i_{0,o}\left(\frac{C_o}{C_{o,ref}}\right)^{\beta}\left[exp\left(\frac{\alpha_a nF}{RT}\eta\right) - exp\left(\frac{\alpha_c nF}{RT}\eta\right)\right] - nFM_{crossover} \tag{8}$$

Subsequently, both V-I and P-I curves could be determined because both the electric potential and the activation overpotentials estimated using Butler-Volmer equation are associated with the local current distribution on the electrode surface which has already obtained through the previous computation.

2.2. Experimental Study

The performance parameters of the hydrogen generator and fuel cell engine are shown in the following.

2.2.1. The Concentration of the KOH

The concentration of the KOH solution can be calculated using the following Eq. (9) [32]–[34].

$$M = \frac{n}{V} \tag{9}$$

where M is molarity (M), n is the number of moles of substance (mol), and v is the volume of solution (L). The mass of KOH can be calculated using the formula in the following Eq. (10) [35], [36].

$$n = \frac{m}{Mr};\ m = n.Mr \tag{10}$$

where n is the number of moles of the substance (mol), m is the mass of the substance (gr), and Mr is the relative molecular mass (gram/mole).

2.2.2. Power Required to Produce H_2

The power required to produce H2 can be calculated using the formula in the following Eq. (11) [37], [38].

$$P_{LH2gen} = V_{H2}.I_{H2} \tag{11}$$

where P_{LH2gen} is the electrical power required by the H_2 generator (W), V_{H2} is the required voltage H_2 generator (V), and I_{H2} is the incoming current H_2 generator (A).

2.2.3. Hydrogen Gas Power

The gas production rate can be calculated using the following Eq. (12) and Eq. (13) [39], [40].

$$\dot{m}_{H2} = \rho_{H2}.Q_{H2} \tag{12}$$

$$P_{H2} = \dot{m}_{H2}.LHV_{H2} \tag{13}$$

where $\dot{m}_{H2}$ is the mass rate of hydrogen gas (Kg/s), ρ_{H2} is the density of hydrogen gas (Kg/m^3), Q_{H2} is hydrogen gas discharge (m^3/s), P_{H2} is hydrogen gas power (W), and LHV_{H2} is the lower heating value (MJ/Kg).

2.2.4. The Efficiency of the H_2 Generator

The H_2 generator can be calculated using the following Eq. (14) [18], [41].

$$\eta_{H2\ Gen} = \frac{P_{H2}}{P_{LH2gen}} \text{ x } 100\ \% \tag{14}$$

where, $\eta_{H2\ Gen}$ is the efficiency of H_2 generator (%), P_{H2} is hydrogen gas power (W), and P_{LH2gen} is electrical power required by the H_2 generator (W).

2.2.5. Hydrogen Power

The gas entering the fuel cell can be calculated using the following Eq. (15) and Eq. (16) [42].

$$\dot{m}_{H2} = \rho_{H2}.Q_{H2} \tag{15}$$

$$P_{H2} = \dot{m}_{H2}.LHV_{H2} \tag{16}$$

where $\dot{m}_{H2}$ is the mass rate of hydrogen gas (Kg/s), ρ_{H2} is the density of hydrogen gas (Kg/m^3), Q_{H2} is hydrogen gas discharge (m^3/s), P_{H2} is hydrogen gas power (W), and LHV_{H2} is the lower heating value (MJ/Kg).

2.2.6. Output Power

Power absorbed by the load can be calculated using the following Eq. (17) [41].

$$P_{L\,FC} = V_{FC}.I_{FC} \tag{17}$$

where $P_{L\,FC}$ is the electric power generated by the fuel cell (W), V_{FC} is the voltage generated by the fuel cell (V), and I_{FC} is the current generated by the fuel cell (A).

2.2.7. The Efficiency of Fuel Cell

The efficiency of the fuel cell can be calculated using the following Eq. (18) [42], [43].

$$\eta_{FC} = \frac{P_{electricity\ FC}}{P_{H2}} \text{ x } 100\% \tag{18}$$

where η_{FC} is the efficiency fuel cell (%), P_{H2} is hydrogen gas power (W), and $P_{L\,fc}$ is electrical power produced by a fuel cell (W).

2.2.8. Specific Fuel Consumption (SFC)

SFC is a measure of the efficiency of a machine that describes the ratio between the amount of fuel consumption and the electrical energy produced. The smaller the SFC value, the better the performance of the machine. SFC can be calculated by the following Eq. (19) [43].

$$SFC = \frac{\dot{m}_{H2}}{P_{LFC}} \tag{19}$$

SFC is specific fuel consumption, ($\frac{Kg}{KWh}$) $\dot{m}_{H2}$ is the mass rate of hydrogen gas ($\frac{Kg}{h}$), and $P_{L\,FC}$ is the electrical power produced by the fuel cell (kW).

2.3. Procedure

Furthermore, the procedure for testing the fuel cell engine using UHP (Ultra High Purity) Hydrogen fuel are as follows: (1) preparing the tools and materials needed for testing and creating test table data; (2) stringing the gas hose from the hydrogen cylinder to the reservoir tube and then to the fuel cell; (3) ensuring that the gas hoses through which the hydrogen gas flows were tightly attached and did not leak by using soap foam; (4) opening the hydrogen regulator valve slowly according to the required pressure; (5) ensuring that all valves to the reservoir were open and the outlet valves to the reservoir were closed; (6) waiting for the required reservoir pressure (1 bar); (7) after the pressure requirement in the reservoir was met, the reservoir output valve slowly was opened; (8) opening the rotameter valve to regulate the hydrogen flow that would enter the fuel cell as needed; (9) the fuel cell would work gradually according to the flow of hydrogen gas; (10) waiting for a while for the fuel cell condition to be ready to be loaded; (11) pressing the load switch on the SCC (Solar Charge Controller); (12) measuring the fuel cell output voltage and current at load 0 using a digital voltampere meter; (13) varying the load (in the form of 10 W and 16 W DC lamps) from 10 W load to the highest load of 60 W; (14) recording the fuel cell voltage and current parameters for each new load addition in the test table; (15) repeating test steps number 8 to number 14 with different variations of hydrogen discharge; (16) after completing taking data on the fuel cell engine, the load was gradually reduced until it reached the zero load position; (17) closing the hydrogen cylinder regulator valve; (18) waiting for the remaining hydrogen in the reservoir to flow into the fuel cell until it run out; (19) closing all valves and valves leading to the fuel cell; (20) cleaning the test equipment and placing it in a safe condition.

Figure 2 presents the procedure for the computational simulation model and experimental testing the fuel cell engine on variations in hydrogen gas fuel flow rate at different electrical loads.

2.4. Experiment of the Fuel Cell Engines

The fuel cell engine test data included output cell voltage, output cell current, hydrogen gas fuel flow rate, specific fuel consumption, and fuel cell output power. The results of applying the fuel cell with the PEM fuel cell is presented in **Figure 3**.

The fuel cell engine equipment and its functions are depicted in **Figure 2**. The names of the fuel cell components are as follows: (1) UHP Hydrogen tube was used to supply hydrogen gas to the fuel cell for the conversion into electrical energy with UHP Hydrogen specifications with a purity level of 99.99%. (2) Hydrogen regulator (pressure regulator) functioned as a distributor and regulated hydrogen gas and stabilized the gas pressure coming out of the tube so that the gas flow became constant, having an output pressure scale specification of 10 bar to 315 bar. (3) The road wheel was used to support the framework of the fuel cell so that it was easy to move. (4) Reservoir hydrogen served to accommodate hydrogen, consisting of one tube with a capacity of 2.5 L reservoir tube body made of acrylic. (5) A hydrogen generator had a dry type specification, or a dry cell was utilized to convert electrolyte solution into hydrogen to be channeled to the fuel cell. (6) A pressure gauge to measure the pressure of hydrogen gas entering the reservoir tube had a pressure scale specification of 0 bar to 6 bar. (7) The hydrogen generator voltmeter was used to measure the voltage generated by the hydrogen generator. (8) Solar Charge Controller (SCC) was used to display voltage and current information on the test equipment connected to the component's output. The fuel cell had a specification of 12 V. (9) The potentiometer was used to adjust the current to turn on the hydrogen fuel generator. (10) The volt-amperemeter cell was used to measure the current and output voltage of the fuel cell with the specifications of measuring DC current 0-10 A and DC Voltage 0-100 V. (11) The lamp load used for the experiment consisted of seven pieces of 10 W and one of 16 W. (12) Pulse Width Modulation (PWM) was used to regulate the size of the current entering the H2 generator with a power requirement specification of 10-50 V DC and a rated current of 60 A. (13) The rotameter was used to measure the flow rate in the form of

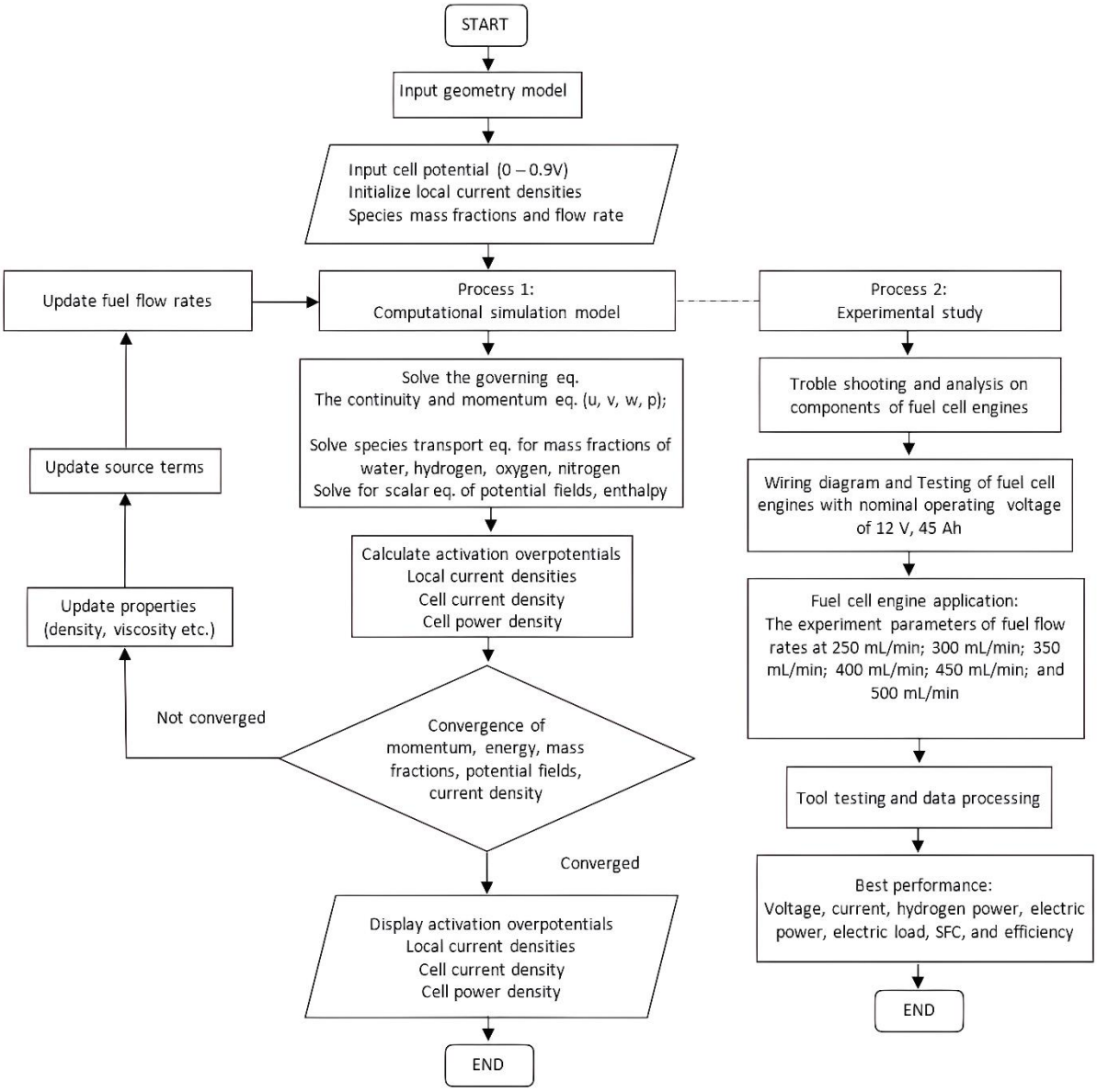

Figure 2. Flowchart for fuel cell performance

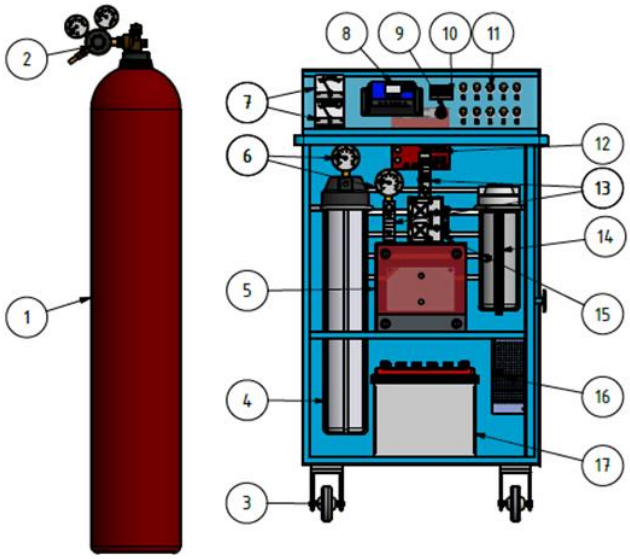

Figure 3. The equipment of fuel cell engines

liquid or gas in a closed tube having a ran specification ge 0-500 mL. (14) A water reservoir was used to accommodate the electrolyte solution to be channeled to the hydrogen generator for the electrolysis process to produce hydrogen. (15) Fuel cells had the function to convert hydrogen into electrical energy with specifications for output performance rated power 150 W. (16) Power supply 220 V functioned as a voltage source entering the hydrogen with a specification of an output voltage of 48 V and a current of 40 A. (17) The battery was used to store electrical power produced by a fuel cell with a specification of 12 V 45 Ah.

Fuel cell test results using UHP (Ultra High Purity) Hydrogen were obtained. This test was carried out by supplying hydrogen from a hydrogen tube with a discharge variation of 250 mL/min. 300 mL/min, 350 mL/min, 400 mL/min, 450 mL/min, and 500 mL/min. In each test of gas discharge variations, the fuel cell was tested by giving a load of 6 DC 12 V 10 W lamps and 1 DC 12 V lamp with 16 W. Test results data Fuel cell using hydrogen tubes are presented in **Table 2**.

3. Result and Discussion

3.1. Simulation Model

Figure 4 show the distributions of hydrogen and oxygen concentrations at the electrode surface at various positions that streams go to the channel outlet, and the inter-diffusion area increases. It is more critical at a 6 mL/min flow rate than at a higher flow rate. **Figure 4** illustrates a larger oxygen supply as the current travels over the cathode's trailing edge once saturation is reached. Nevertheless, diffusion of oxygen in the channel enables oxygen absorption to spread swiftly across the microchannels beyond the streaming edge of the electrode.

The concentration supply over the electrode within the channel, as seen in **Figure 4**, appears to represent the formation of the depleted interface layer among the fuel and oxidant streams over the electrode at a volumetric flow rate of 6 mL/min along the channel. This is due to a decline in the microchannel flow rate, which results in a low concentration fuel zone. Fuel loss comes from the swiftly rising torrent in the anode channel at a high volumetric flow rate of 30 mL/min. A depleted boundary layer forms along the microchannel for the overall fuel depletion across anode porous electrodes. As seen in **Figure 5**, the local current density takes a pinnacle at the electrode edge around the channel's midpoint, with two distinctive anode permeability.

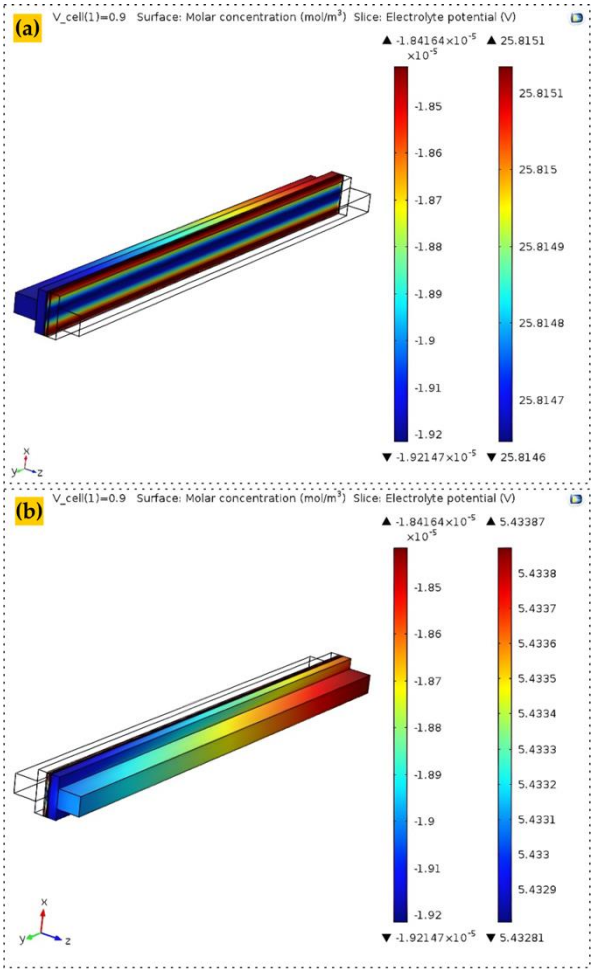

Figure 4. (a) Anode hydrogen concentration; (b) Cathode hydrogen concentration 0.05-M at 0.5 ml/min

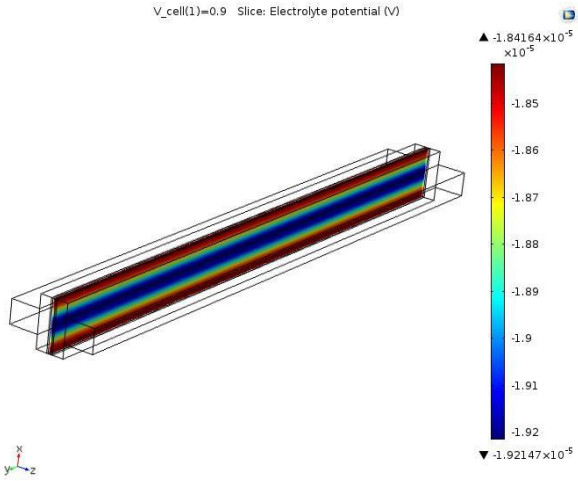

Figure 5. Membrane current density

Table 2. Experimental test results in data fuel cell using UHP (Ultra High Purity)

Discharge (mL/s)	Discharge (mL/min)	Load (Watts)	Voltage (V)	Current (A)
4.167	250	0	18.20	0.00
		10	16.30	1.15
		16	16.30	1.17
		20	14.70	2.10
		26	14.70	2.14
		30	10.70	2.56
		36	10.60	2.65
		40	7.20	2.77
		46	7.10	2.79
		50	5.10	2.80
		60	5.00	2.82
5.00	300	0	18.30	0 ,00
		10	16.40	1.15
		16	16.40	1.17
		20	14.80	2.10
		26	14.70	2.14
		30	11.20	2.60
		36	11.20	2.62
		40	7.40	2, 83
		46	7.40	2.85
		50	5.30	2.88
		60	5.20	2.89
5.83	350	0	18.40	0.00
		10	16.40	1.15
		16	16.40	1.17
		20	14, 70	2.12
		26	14.70	2.14
		30	11.30	2.62
		36	11.20	2.63
		40	7.50	2.85
		46	7.50	2.86
		50	5.20	2.88
		60	5.20	2.89
6.67	400	0	18.50	0.00
		10	16.30	1.15
		16	16.10	1.17
		20	14.60	2.10
		26	14.60	2.14
		30	11.50	2.64
		36	11.40	2.65
		40	7.70	2.87
		46	7.60	2.89
		50	5.40	2.92
		60	5.30	2.94
7.50	450	0	18.50	0.00
		10	16.40	1 ,15
		16	16,40	1.17
		20	14.90	2.12
		26	14.80	2.15
		30	11.40	2.65
		36	11.40	2.66
		40	7.60	2.89
		46	7.60	2, 90
		50	5.40	2.92
		60	5.30	2.94
8.33	500	0	18.50	0.00
		10	15.80	1.14
		16	15.80	1.15
		20	14.60	2.07
		26	14, 20	2.14
		30	11.50	2.67
		36	11.40	2.67
		40	7.70	2.89
		46	7.60	2.91
		50	5.40	2.92
		60	5.40	2.95

The change in local current density on the electrode surface becomes noticeable as the flow rate increases. Changes in the local current density at the surface of the electrode become apparent as the flow rate increases due to the diffusion limit of the fuel concentration in the cell channel. The depletion boundary layer caused by the fuel consumption over the anode electrode. The stream rapidly replenishes depletion of the fuel while the formation of the region with a low fuel concentration due to decreasing of the volumetric flow rates. While the fuel concentration distribution of the very low volumetric flow rate that shows that the growth of the depletion layer on electrode surface inside the cell channel seems obvious. While the volumetric flow rate of 250 mL/min, 300 mL/min, 350 mL/min, 400 mL/min, 450 mL/min and 500 mL/min diffusion of fuel is clearly visible in the cell channel interface or the middle of the channel, where the fuel across and reach the cathode side through stream in the cell channel. The model takes into account the diffusion limits and electrochemical reactions without ohmic drop restrictions and was performed numerically for the three active layer geometric descriptions using the finite element method. Diffusion limitation within the entire active layer has been confirmed, but effects of diffusion and competition at the particle level have also been demonstrated. As a practical conclusion, this effect at the particle level, is almost negligible for the reduction of oxygen, significantly affecting the oxidation of hydrogen. Due to diffusion limitations that prohibit the reaction on the surface from being completely exploited, the local current density on the surface of the cathode catalyst layer decreases than on the surface of the anode catalyst layer. Local current density is low at the entry, steadily rises in the flow channel's middle, and finally decreases towards the outflow. The cell performance is more significant in the intake area, corresponding to increased electrolyte conductivity (lower ohmic overvoltage).

3.2. Experimental Result

The result of this study was that the maximum output current generated by the fuel cell was 3.97 A at 3.75 mL/s with a discharge gas at a load of 60 W. Meanwhile, the most significant output voltage generated by the fuel cell was 17.7 V, with a discharge gas of 3.75 mL/s without loading.

Figure 6 shows that the more current in the load, the lower the output voltage produced. It is due to losses in the voltage, i.e., the activation voltage loss, and the resistance voltage loss. In this case, the output voltage fuel cell is strongly influenced by changes in the connected load.The greater the load current, the lower the fuel cell. In addition, the greater the hydrogen flow rate, the greater the generated voltage and current. In this study, the highest voltage obtained was 18.50 Volt at load 0 with a flow rate of 500 mL/min.

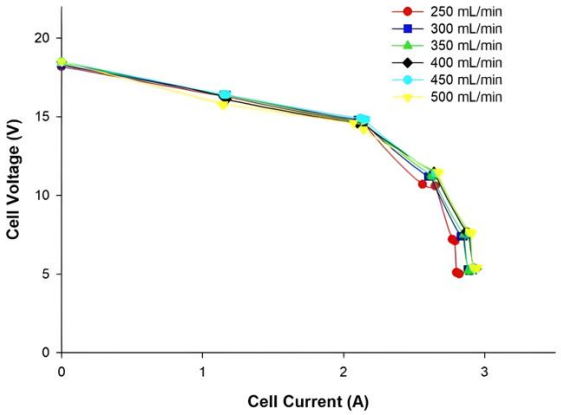

Figure 6. The characteristics of the output current of the fuel cell and the cell voltage with different hydrogen gas discharge (250 mL/min; 300 mL/min; 350 mL/min; 400 mL/min; 450 mL/min; 500 mL/min)

An example was taken in the test with a gas discharge of 250 mL/min, and there was a voltage loss due to the activation of the zero voltage (without load) of 18.20 V, which decreased to 16.30 V at the first loading, i.e., the lamp load of 10 W. It was due to the voltage loss—required to remove the ion from the electrode where the ion was formed. Meanwhile, the voltage loss due to activation occurred at the 2nd to 10th loadings. Besides, the resistance of voltage loss was the product of the current flow and the resistance in the cell. During loading, the voltage loss due to resistance would increase.

The fuel cell output power fuel cell tended to increase and then decrease (fluctuating). The problem with operating the fuel cell system is maintenance fuel cell output voltage. The fuel cell output voltage can be explained from the V-I characteristics or known as the polarization of the fuel cell used. The characteristics of the output voltage of the fuel cell are strongly influenced by changes in load. The greater the load current, the lower the output voltage of the fuel cell will be.

This characteristic of the fuel cell makes it difficult to maintain the output voltage of the fuel cell at a certain constant value. The characteristics of the output voltage to the load current from the fuel cell are shown in **Figure 6** and **Figure 7**. The condition of the output voltage of the fuel cell that is not constant will be a problem when the fuel cell is connected to a load in the form of electronic equipment. This is because usually electronic equipment has a certain working voltage so that if it exceeds the working voltage threshold, the equipment will be damaged and if the voltage supplied by the fuel cell is less than the working voltage, the equipment cannot work optimally. Output fuel cell power in the **Figure 6** was 31.8 W with a hydrogen gas discharge of 450 mL/min, and the fuel cell was 2.95 A at a hydrogen gas discharge of 500 mL/min. The resulting current increased as the load increased, but the voltage decreased in **Figure 3**. In addition, the output power produced by the fuel cell was the product of the fuel cell's output voltage and the fuel cell's output current. Thus, the power output value of the fuel cell was influenced by the voltage value and current that changed with the addition of hydrogen gas discharge.

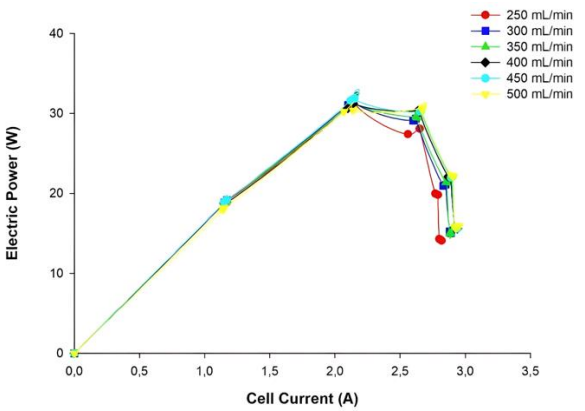

Figure 7. The characteristics of the fuel cell current and the electric power with different hydrogen gas discharges (250 mL/min; 300 mL/min; 350 mL/min; 400 mL/min; 450 mL/min; 500 mL/min)

Figure 6 and **Figure 7** show that as the load current increased, the fuel cell decreased. The output fuel cell power in the **Figure 6**, 31.8 W, occurred at 250 mL/min hydrogen gas discharge. The highest current was 2.95 A, while the highest voltage was 18.5 V. The voltage drop was caused by voltage losses, namely voltage losses due to resistance. Then, the more significant the current issued by the fuel cell, the greater the power generated. However, the increase in power that occurred was not too significant. The power in the **Figure 7** was also obtained from the product of the fuel cell. Hence, even though the output current increased with increasing load because the voltage decreased, the electrical power produced was not constantly increasing.

The optimal value for the output power was 31.8 W at the most significant gas supply, which was 450 mL/min, in **Figure 8**. In comparison, the highest efficiency was obtained at 69.8% at the smallest hydrogen gas discharge, which was 250 mL/min. Based on the Eq. 1 to Eq. 4, represent that the amount of current fuel cell generated on the anode electrode depends on the fuel concentration. In addition, at a low flow rate and a lower fuel concentration on the anode electrode surface leading to low power density due to having the low open circuit voltage. Fuel utilization can be presented as:

$$\varepsilon_{fuel} = \frac{I}{nFQ_{fuel}} \tag{17}$$

In here, I is the current generated by the fuel cell at 0.7 V, n is number of transferred electrons at the electrode (n = 2), is the Faraday constant (F = 96485 C/mol), Q_{fuel} represents the fuel rate which is supplied to the fuel cell in unit of mol/s. **Figure 8** shows performance fuel cell between efficiency of fuel cell and electric power under different conditions of volumetric flow rate which have affected by raising the volumetric flow rate ranging from 250 mL/min, 300 mL/min, 350 mL/min, 400 mL/min, 450 mL/min, and 500 mL/min. At a higher flow rate will increase power density because the lower mixed voltage at the cathode side can generate a higher voltage. Besides the influence of the higher availability of reactant on the electrode surface active area and a higher volumetric flow rate of the electrochemical reaction can increase the current generated by the fuel cell. Based on the cell performance of the experiment and numerical simulation, which were the maximum electric power of the fuel cell always occurred at a voltage between 0.3 V and 0.7 V, the faster sharp drop of voltage in V-I curve at a higher volumetric flow rate to lower flow rate, which was 250 mL/min, 300 mL/min, 350 mL/min, 400 mL/min, 450 mL/min, and 500 mL/min at 0.7 V.

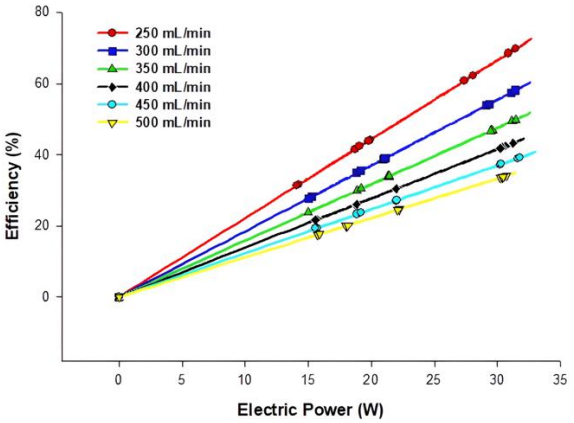

Figure 8. The characteristics of the electric power and the fuel cell efficiency with different hydrogen gas discharges (250 mL/min; 300 mL/min; 350 mL/min; 400 mL/min; 450 mL/min; 500 mL/min)

Moreover, the output power produced was influenced by the fuel cell's output voltage and output current. It is known from **Figure 7** that the greater the output power of the fuel cell, the greater the efficiency value. It means that the relationship between the value of efficiency and output power is directly proportional. It was also found that the more significant the variation of hydrogen gas discharge, the smaller the efficiency value. This efficiency value was also influenced by the increased input power entering the fuel cell. However, the optimal output power value for each variation of hydrogen gas discharge was only up to 26 W load, and then the output power value decreased. It suggests that the PEM Fuel Cell's performance was optimal at the output power and efficiency value. The value of the output power increasing from a load of 10 W to a load of 26 W and then decreasing from a load of 36 W to a load of 60 W. Meanwhile, the value of SFC decreased with time. With an increase in the output power, the value of SFC increased when the value of the output power decreased. It denotes that the relationship between the output power with SFC is inversely proportional. In the second loading on each variation of the hydrogen gas discharge, the SFC value spiked and then decreased along with the increase in the output power of the fuel cell. In other words, the smaller the SFC value, the better the machine's performance. In addition, fuel cells will achieve the best performance at optimal load. In this study, it is known that the optimal SFC value at the input hydrogen gas discharge was 250 mL/min, and the output power was 31.588 W.

Changes in load gave a swift reaction to the changes in the fuel cell, which decreased when given a more significant load. Then, it was also influenced by the changes in the output current of the fuel cell, which got more prominent as the load was added. **Figure 9** also indicates that the optimum output power of the fuel cell was when the lamp load was 26 W. For example, the optimum output power produced by the fuel cells was the largest, 31.8 W, at a hydrogen gas discharge of 450 mL/min. It is because the fuel cell output power is the product of the output voltage and the fuel cell output current.

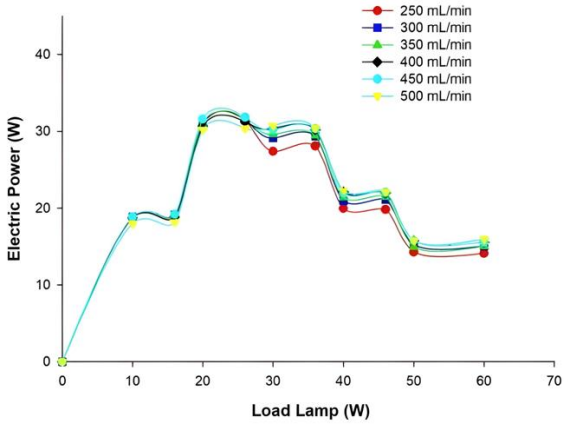

Figure 9. The characteristics of a load of the lamp and the electric power with different hydrogen gas discharges (250 mL/min; 300 mL/min; 350 mL/min; 400 mL/min; 450 mL/min; 500 mL/min)

Changes in load gave a swift reaction to changes in the fuel cell, which decreased when given a more significant load, in **Figure 10**. Then, it was also influenced by changes in the fuel cell, which got more prominent as the load was added. The figure also shows the optimum output power of the fuel cell when the lamp load was 26 W. For example, the fuel cell's most significant optimum output power was 31.8 W at a hydrogen gas discharge of 450 mL/min. It is because the fuel cell is the product of the output voltage and the fuel cell. The increasing concentration of KOH solution in the electrolyzer causes the electrolyte solution to flow more and more electric current, so that the water molecules that decompose into hydrogen gas is increasing and the electrical energy consumed can be optimally used for the electrolysis of water. But after reaching the maximum point, the increase in hydrogen gas production is smaller than the increase in the required electrical energy, which is caused by the

greater amount of electrical energy flowing in the electrolysis circuit, the more electrical energy that turns into heat that is released into the environment. This results in a decrease in the efficiency of the electrolyzer, which will result in a decrease in efficiency. While the value of efficiency in giving variations The greater the hydrogen gas discharge, the smaller the efficiency value at the same load. The efficiency value is also affected by the increase in load from 10 W - 60 W, the increase in input power entering the fuel cell and the output power.

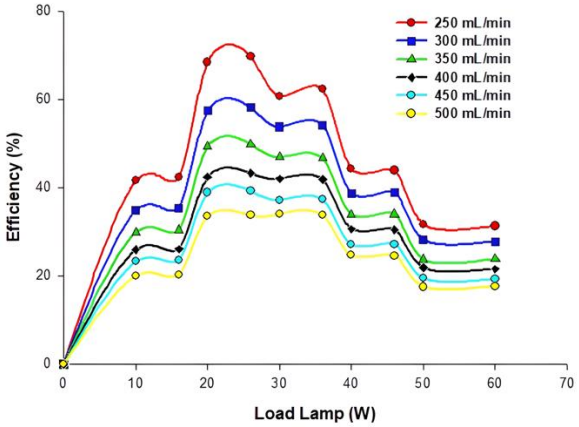

Figure 10. The characteristics of a load of the lamp and the efficiency with different hydrogen gas discharges (250 mL/min, 300 mL/min, 350 mL/min, 400 mL/min, 450 mL/min, and 500 mL/min)

Specific fuel consumption is defined as the amount of hydrogen gas used per hour to produce each kW of engine power. Based on **Figure 11**, it is shown the specific fuel consumption against the load function on fuel consumption at fuel flow rates of 250 mL/min, 300 mL/min, 350 mL/min, 400 mL/min, 450 mL/min, and 500 mL/min have the same trendline. The specific fuel consumption (kg/kWh) decreases when the load is increased (20 W), and then increases again when the fuel cell engine is given a load of up to 60 W. The higher the load, the consumption of hydrogen gas fuel will also increase. This is because at a high load there is a greater loss of heat in chemical reactions so that fuel consumption will also increase. The phenomenon indicates that the PEM Fuel Cell has the best performance at a load of 26 W. It is also known that the smallest SFC value was 0.042918 kg/kWh at the smallest gas input discharge of 250 mL/min. Moreover, the addition of hydrogen gas flow rate at each of the same loads showed that the greater the flow rate was given, the greater the SFC PEM Fuel Cell was reached. When the fuel cell engine is at a low discharge flow rate, the longer time required per cycle causes higher heat loss to the heat-producing chemical processes and fuel consumption slowly increases. Consumption of hydrogen gas fuel is also affected by the chemical reaction process of hydrogen and oxygen gas that passes through the fuel cell membrane. Specific fuel consumption is low when the flow rates of hydrogen gas and air are at stoichiometric conditions or fuel equivalent ratios. Furthermore, knowing the SFC value is one way to determine an engine's performance. SFC is also a measure of the efficiency of an engine that describes the ratio between the amount of fuel consumption and the electrical energy produced. The smaller the SFC value, the better the performance of a machine.

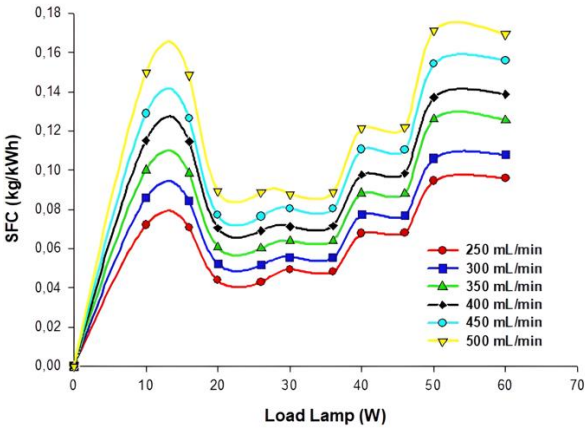

Figure 11. The characteristics of a load of the lamp and the specific fuel consumption (SFC) with different hydrogen gas discharges (250 mL/min; 300 mL/min; 350 mL/min; 400 mL/min; 450 mL/min; 500 mL/min)

4. Conclusion

This study investigates the application of a PEM fuel cell engine through a simulation study of the PEM fuel cell model and experimentally through testing a fuel cell engine. A three-dimensional flow simulation of a PEM fuel cell has been presented. Computational analysis of the model shows how to modify a fuel cell to incorporate the required electrochemical processes. The diffusion layers at the anode and cathode show a significant difference from studies that do not include the diffusion layer. This work experimentally also describes the consumption behavior of hydrogen gas by analyzing the fuel flow rate. The effect of the diffusion layer added

to both sides of the MEA will result in a larger reaction area. However, the diffusion layer creates a flow resistance and therefore, our study shows a decrease in the local current density relative to the hydrogen gas fuel flow rate. The performance results of the PEM Fuel Cell for the flow rate of hydrogen gas fuel from the electrolyzer are obtained by producing hydrogen gas by electrolysis to supply the PEM Fuel Cell engine, so that the engine can work to convert chemical energy into electrical energy in the fuel cell engine. In other words, the higher the solution concentration and the input current, the higher the gas produced. Nevertheless, hydrogen gas production by electrolysis to power the PEM Fuel Cell engine was not optimal with the quality and requirements, so the engine could not work optimally to convert up into electrical energy. Then, PEM Fuel Cell was modified from a nominal operating voltage of 2.3-3 V to PEM Fuel Cell with a nominal operating voltage of 18 V. Afterward, the testing using UHP hydrogen obtained a maximum efficiency of 69.8% at the smallest hydrogen gas discharge, 250 mL/min. Thus, the optimal PEM fuel cell engine was at 26 W load with the best specific fuel consumption of 0.0429 kg/kWh.

Acknowledgements

This research was funded by the Ministry of Education, Culture, Research and Technology of Indonesia, grant number 157/SPK/D.D4/PPK.01.APTV/VI/2023 and P3M Politeknik Negeri Semarang, grant number 457/PL4.7.2/PT/2023. The authors are indebted to the Ministry of Science and Technology of Taiwan for the funding under the contract of MOST 108-2628-E-992-001-MY3.

Author's Declaration

Authors' contributions and responsibilities

The authors made substantial contributions to the conception and design of the study. The authors took responsibility for data analysis, interpretation, and discussion of results. The authors read and apporved the final manuscrips.

Funding

As explained in the acknowledgments section.

Availability of data and materials

All data are available from the authors.

Competing interests

The authors declare no competing interest.

Additional information

No additional information from the authors.

References

[1] A. L. Dicks, "4.08 - PEM Fuel Cells: Applications," T. M. B. T.-C. R. E. (Second E. Letcher, Ed. Oxford: Elsevier, 2022, pp. 232–260.

[2] T. B. Ferriday and P. H. Middleton, "4.07 - Alkaline Fuel Cells, Theory and Applications," T. M. B. T.-C. R. E. (Second E. Letcher, Ed. Oxford: Elsevier, 2022, pp. 166–231.

[3] P. Kumar, "4.14 - Future Perspective on Hydrogen and Fuel Cells," T. M. B. T.-C. R. E. (Second E. Letcher, Ed. Oxford: Elsevier, 2022, pp. 379–398.

[4] Y. D. Herlambang, F. Arifin, T. Prasetyo, and A. Roihatin, "Numerical analysis of phenomena transport of a proton exchange membrane (PEM) fuel cell," *Journal of Advanced Research in Fluid Mechanics and Thermal Sciences*, vol. 80, no. 2, pp. 127–135, 2021, doi: 10.37934/arfmts.80.2.127135.

[5] P. Ahmadi and A. Khoshnevisan, "Dynamic simulation and lifecycle assessment of hydrogen fuel cell electric vehicles considering various hydrogen production methods," *International Journal of Hydrogen Energy*, vol. 47, no. 62, pp. 26758–26769, 2022, doi: 10.1016/j.ijhydene.2022.06.215.

[6] M. Hasani and N. Rahbar, "Application of thermoelectric cooler as a power generator in waste heat recovery from a PEM fuel cell–an experimental study," *International Journal of Hydrogen Energy*, vol. 40, no. 43, pp. 15040–15051, 2015, doi: 10.1016/j.ijhydene.2015.09.023.

[7] Y. D. Herlambang, A. Roihatin, and F. Arifin, "Model experimental of photovoltaic-electrolyzer fuel cells as a small-scale power," in *International Conference on Vocational Education of Mechanical and Automotive Technology*, 2020, vol. 1700, no. 1, p. 12100, doi: 10.1088/1742-6596/1700/1/012100.

[8] D. Rašić and T. Katrašnik, "Multi-domain and Multi-scale model of a fuel cell electric vehicle to predict the effect of the operating

conditions and component sizing on fuel cell degradation," *Energy Conversion and Management*, vol. 268, p. 116024, 2022, doi: 10.1016/j.enconman.2022.116024.

[9] H. Lan, D. Hao, W. Hao, and Y. He, "Development and comparison of the test methods proposed in the Chinese test specifications for fuel cell electric vehicles," *Energy Reports*, vol. 8, pp. 565–579, 2022, doi: 10.1016/j.egyr.2022.02.006.

[10] U. Lee, S. Jeon, and I. Lee, "Design for shared autonomous vehicle (SAV) system employing electrified vehicles: Comparison of battery electric vehicles (BEVs) and fuel cell electric vehicles (FCEVs)," *Cleaner Engineering and Technology*, vol. 8, p. 100505, 2022, doi: 10.1016/j.clet.2022.100505.

[11] Z. Song, Y. Pan, H. Chen, and T. Zhang, "Effects of temperature on the performance of fuel cell hybrid electric vehicles : A review," *Applied Energy*, vol. 302, no. April, p. 117572, 2021, doi: 10.1016/j.apenergy.2021.117572.

[12] G. Şefkat and M. A. Özel, "Experimental and numerical study of energy and thermal management system for a hydrogen fuel cell-battery hybrid electric vehicle," *Energy*, vol. 238, p. 121794, 2022, doi: 10.1016/j.energy.2021.121794.

[13] Y. D. Herlambang, J. Shyu, and S. Lee, "Numerical simulation of the performance of air-breathing direct formic acid microfluidic fuel cells," *Micro & Nano Letters*, vol. 12, no. 11, pp. 860–865, 2017, doi: 10.1049/mnl.2017.0322.

[14] D. Zhou, F. Gao, A. Al-Durra, E. Breaz, A. Ravey, and A. Miraoui, "Development of a multiphysical 2-D model of a PEM fuel cell for real-time control," *IEEE Transactions on Industry Applications*, vol. 54, no. 5, pp. 4864–4874, 2018, doi: 10.1109/TIA.2018.2839082.

[15] Y. D. Herlambang, S.-C. Lee, and H.-C. Hsu, "Numerical estimation of photovoltaic–electrolyzer system performance on the basis of a weather database," *International Journal of Green Energy*, vol. 14, no. 7, pp. 575–586, 2017, doi: 10.1080/15435075.2017.1307200.

[16] I. Khazaee and A. Rava, "Numerical simulation of the performance of solid oxide fuel cell with different flow channel geometries," *Energy*, vol. 119, pp. 235–244, 2017, doi: 10.1016/j.energy.2016.12.074.

[17] S. Thomas, S. S. Araya, S. H. Frensch, T. Steenberg, and S. K. Kær, "Hydrogen mass transport resistance changes in a high temperature polymer membrane fuel cell as a function of current density and acid doping," *Electrochimica Acta*, vol. 317, pp. 521–527, 2019, doi: 10.1016/j.electacta.2019.06.021.

[18] W. Li *et al.*, "Experimental and numerical analysis of a three-dimensional flow field for PEMFCs," *Applied Energy*, vol. 195, pp. 278–288, 2017, doi: 10.1016/j.apenergy.2017.03.008.

[19] T. Berning and N. Djilali, "Three-dimensional computational analysis of transport phenomena in a PEM fuel cell—a parametric study," *Journal of Power Sources*, vol. 124, no. 2, pp. 440–452, 2003, doi: 10.1016/S0378-7753(03)00816-4.

[20] S. Haji, "Analytical modeling of PEM fuel cell i–V curve," *Renewable Energy*, vol. 36, no. 2, pp. 451–458, 2011, doi: 10.1016/j.renene.2010.07.007.

[21] M. H. Eikani, A. Eliassi, N. Khandan, and V. R. Nafisi, "Design and fabrication of a 300W PEM fuel cell test station," *Procedia Engineering*, vol. 42, pp. 368–375, 2012, doi: 10.1016/j.proeng.2012.07.428.

[22] X.-D. Wang, W.-M. Yan, W.-C. Won, and D.-J. Lee, "Effects of operating parameters on transport phenomena and cell performance of PEM fuel cells with conventional and contracted flow field designs," *International Journal of Hydrogen Energy*, vol. 37, no. 20, pp. 15808–15819, 2012, doi: 10.1016/j.ijhydene.2012.02.145.

[23] Y. D. Herlambang, S.-C. Lee, J.-C. Shyu, and C.-J. Liu, "Numerical study and modeling of the solar radiation measurement on tilted surface for the local behavior database," *Journal of the Chinese Society of Mechanical Engineers*, vol. 37, no. 5, pp. 441–448, 2016, doi: 10.5297/ser.1201.002.

[24] H. Sun, C. Xie, H. Chen, and S. Almheiri, "A numerical study on the effects of temperature and mass transfer in high temperature PEM fuel cells with ab-PBI membrane," *Applied Energy*, vol. 160, pp. 937–944, 2015, doi: 10.1016/j.apenergy.2015.02.053.

[25] Y. D. Herlambang, K. Kurnianingsih, A. Roihatin, T. Prasetyo, M. Marliyati, and F.

Arifin, "Experimental and Numerical Analysis of Low Temperature Proton Exchange Membrane Fuel Cell (PEMFC) with Different Fuel Flow Rate in Improving Fuel Cell Performance," *Key Engineering Materials*, vol. 924, pp. 153–166, 2022, doi: 10.4028/p-5jbb8o.

[26] B. Najafi, A. H. Mamaghani, F. Rinaldi, and A. Casalegno, "Fuel partialization and power/heat shifting strategies applied to a 30 kWel high temperature PEM fuel cell based residential micro cogeneration plant," *International Journal of Hydrogen Energy*, vol. 40, no. 41, pp. 14224–14234, 2015, doi: 10.1016/j.ijhydene.2015.08.088.

[27] S.-W. Ham, S.-Y. Jo, H.-W. Dong, and J.-W. Jeong, "A simplified PEM fuel cell model for building cogeneration applications," *Energy and Buildings*, vol. 107, pp. 213–225, 2015, doi: 10.1016/j.enbuild.2015.08.023.

[28] S. Authayanun, K. Im-Orb, and A. Arpornwichanop, "A review of the development of high temperature proton exchange membrane fuel cells," *Chinese Journal of Catalysis*, vol. 36, no. 4, pp. 473–483, 2015, doi: 10.1016/S1872-2067(14)60272-2.

[29] Y. Devrim, H. Devrim, and I. Eroglu, "Development of 500 W PEM fuel cell stack for portable power generators," *International Journal of Hydrogen Energy*, vol. 40, no. 24, pp. 7707–7719, 2015, doi: 10.1016/j.ijhydene.2015.02.005.

[30] S. Rezazadeh, H. Sadeghi, R. Mirzaei, and I. Mirzaei, "Numerical Investigation of Flow Channel Geometrical Configuration Design Effect on a Proton Exchange Membrane Fuel Cell Performance and Mass Transport Phenomenon," in *2018 2nd International Conference on Smart Grid and Smart Cities (ICSGSC)*, 2018, pp. 137–141, doi: 10.1109/ICSGSC.2018.8541298.

[31] P. T. Nguyen, T. Berning, and N. Djilali, "Computational model of a PEM fuel cell with serpentine gas flow channels," *Journal of Power Sources*, vol. 130, no. 1–2, pp. 149–157, 2004, doi: 10.1016/j.jpowsour.2003.12.027.

[32] S. Deng, M. K. Hassan, K. A. Mauritz, and J. W. Mays, "Hydrocarbon-based fuel cell membranes: Sulfonated crosslinked poly (1, 3-cyclohexadiene) membranes for high temperature polymer electrolyte fuel cells," *Polymer*, vol. 73, pp. 17–24, 2015, doi: 10.1016/j.polymer.2015.07.030.

[33] Y. D. Herlambang *et al.*, "A Numerical Study of Bubble Blockage in Microfluidic Fuel Cells," *Processes*, vol. 10, no. 5, p. 922, 2022, doi: 10.3390/pr10050922.

[34] W. J. Yang, H. Y. Wang, and Y. B. Kim, "Channel geometry optimization using a 2D fuel cell model and its verification for a polymer electrolyte membrane fuel cell," *International Journal of Hydrogen Energy*, vol. 39, no. 17, pp. 9430–9439, 2014, doi: 10.1016/j.ijhydene.2014.03.243.

[35] L. Rostami, P. M. G. Nejad, and A. Vatani, "A numerical investigation of serpentine flow channel with different bend sizes in polymer electrolyte membrane fuel cells," *Energy*, vol. 97, pp. 400–410, 2016, doi: 10.1016/j.energy.2015.10.132.

[36] R. E. Rosli *et al.*, "A review of high-temperature proton exchange membrane fuel cell (HT-PEMFC) system," *International Journal of Hydrogen Energy*, vol. 42, no. 14, pp. 9293–9314, 2017, doi: 10.1016/j.ijhydene.2016.06.211.

[37] R. K. A. Rasheed, Q. Liao, Z. Caizhi, and S. H. Chan, "A review on modelling of high temperature proton exchange membrane fuel cells (HT-PEMFCs)," *International journal of hydrogen energy*, vol. 42, no. 5, pp. 3142–3165, 2017, doi: 10.1016/j.ijhydene.2016.10.078.

[38] D. R. Dekel, "Review of cell performance in anion exchange membrane fuel cells," *Journal of Power Sources*, vol. 375, pp. 158–169, 2018, doi: 10.1016/j.jpowsour.2017.07.117.

[39] Y. D. Herlambang, A. Roihatin, K. Kurnianingsih, T. Prasetyo, S.-C. Lee, and J.-C. Shyu, "Computation and numerical modeling of fuel concentration distribution and current density on performance of the microfluidic fuel cell," in *AIP Conference Proceedings*, 2020, vol. 2197, no. 1, doi: 10.1063/1.5140949.

[40] K. Nikiforow, P. Koski, and J. Ihonen, "Discrete ejector control solution design, characterization, and verification in a 5 kW PEMFC system," *International Journal of Hydrogen Energy*, vol. 42, no. 26, pp. 16760–16772, 2017, doi: 10.1016/j.ijhydene.2017.05.151.

[41] A. Muchtar, N. A. M. N. Aman, M. R.

Somalu, M. I. Rosli, and N. S. Kalib, "Overview of Computational Fluid Dynamics Modelling in Solid Oxide Fuel Cell," *Journal of Advanced Research in Fluid Mechanics and Thermal Sciences*, vol. 52, no. 2, pp. 174–181, 2018.

[42] M. R. Somalu, N. W. Norman, and A. Muchtar, "A short review on the proton conducting electrolytes for solid oxide fuel cell applications," *Journal of Advanced Research in Fluid Mechanics and Thermal Sciences*, vol. 52, no. 2, pp. 115–122, 2018.

[43] Y. D. Herlambang, A. Roihatin, S.-C. Lee, and J.-C. Shyu, "MEMS-Based Microfluidic fuel cell for in situ analysis of the cell performance on the electrode surface," in *Journal of Physics: Conference Series*, 2020, vol. 1444, no. 1, p. 12044, doi: 10.1088/1742-6596/1444/1/012044.